



Published in final edited form as:

Brain Struct Funct. 2021 December ; 226(9): 2777–2791. doi:10.1007/s00429-021-02385-7.

Morphological evidence for multiple distinct channels of corticogeniculate feedback originating in mid-level extrastriate visual areas of the ferret

Matthew Adusei¹, J. Michael Hasse², Farran Briggs^{1,3,4,5,6}

¹Neuroscience Graduate Program, University of Rochester Medical Center, 601 Elmwood Ave. Box 603, Rochester, NY 14642, USA

²Center for Neural Science, New York University, New York, NY 10003, USA

³Department of Neuroscience, University of Rochester School of Medicine, Rochester, NY 14642, USA

⁴Department of Brain and Cognitive Sciences, University of Rochester, Rochester, NY 14627, USA

⁵Ernest J. Del Monte Institute for Neuroscience, University of Rochester School of Medicine, Rochester, NY 14642, USA

⁶Center for Visual Science, University of Rochester, Rochester, NY 14627, USA

Abstract

Complementary reciprocal feedforward and feedback circuits connecting the visual thalamus with the visual cortex are essential for visual perception. These circuits predominantly connect primary and secondary visual cortex with the dorsal lateral geniculate nucleus (LGN). Although there are direct geniculocortical inputs to extrastriate visual cortex, whether reciprocal corticogeniculate neurons exist in extrastriate cortex is not known. Here we utilized virus-mediated retrograde tracing to reveal the presence of corticogeniculate neurons in three mid-level extrastriate visual cortical areas in ferrets: PMLS, PLLS, and 21a. We observed corticogeniculate neurons in all three extrastriate areas, although the density of virus-labeled corticogeniculate neurons in extrastriate cortex was an order of magnitude less than that in areas 17 and 18. A cluster analysis of morphological metrics quantified following reconstructions of the full dendritic arborizations of virus-labeled corticogeniculate neurons revealed six distinct cell types. Similar corticogeniculate cell types to those observed in areas 17 and 18 were also observed in PMLS, PLLS, and 21a. However, these unique cell types were not equally distributed across the three extrastriate areas. The majority of corticogeniculate neurons per cluster originated in a single area, suggesting unique parallel organizations for corticogeniculate feedback from each extrastriate area to the LGN. Together, our findings demonstrate direct feedback connections from mid-level extrastriate

[✉]Farran Briggs, farran_briggs@urmc.rochester.edu.
Author contributions

M.A. and F.B. designed the study. J.M.H. and F.B. collected the data. J.M.H. performed histological processing. M.A. analyzed the data. M.A. and F.B. wrote the manuscript.

Conflict of interest The authors declare no competing financial interests.

visual cortex to the LGN, supporting complementary reciprocal circuits at multiple processing stages along the visual hierarchy. Importantly, direct reciprocal connections between the LGN and extrastriate cortex, that bypass V1, could provide a substrate for residual vision following V1 damage.

Keywords

Corticogeniculate; LGN; PMLS; PLLS; Area 21a; Feedback

Introduction

Sensory processing areas are reciprocally interconnected via feedforward and feedback circuits whose complementary activities are essential for sensory perception. In the visual system, feedforward circuits that relay information from the retina through the visual thalamus, the dorsal lateral geniculate nucleus (LGN), to the primary visual cortex (V1) are complemented by corticogeniculate circuits that connect V1 to the LGN in the feedback direction (Briggs 2020). The visual cortex is hierarchically organized into anatomically and physiologically distinct areas that are also interconnected via feedforward and feedback corticocortical circuits (Felleman and Van Essen 1991). Within the hierarchy, V1 serves as a critical gateway, as almost all visual signals from the LGN pass through V1 before reaching mid-level extrastriate visual areas such as the middle temporal area (MT) and V4 (Felleman and Van Essen 1991). However, when V1 is damaged, some residual vision, including motion sensitivity, remains, a phenomenon known as blindsight (Weiskrantz 2009). Residual vision in blindsight may be explained by direct connections between subcortical areas and extrastriate visual cortex that bypass V1 (Cowey 2010). In support of this notion, neuroanatomical tracing studies in primates and carnivores have found sparse direct feedforward connections from the LGN to extrastriate visual areas, including primate V4 and MT and homologous areas 21a and PMLS in ferrets and cats (Dell et al. 2018; Lyon and Rabideau 2012; Lysakowski et al. 1988; Sherk 1986; Sincich et al. 2004; Tong et al. 1982). Additionally, physiological studies in primates and carnivores show that residual visual activity remains in extrastriate visual areas following V1 cooling or lesions (Azzopardi et al. 2003; Girard et al. 1992; Jayakumar et al. 2013; Michalski et al. 1993; Rodman et al. 1989; Rosa et al. 2000; Schmid et al. 2010). Given that visual perception likely relies on complementary feedforward and feedback circuits at each processing level, we predicted that direct geniculocortical inputs to extrastriate visual areas are complemented by reciprocal corticogeniculate circuits. We therefore searched for the presence of corticogeniculate neurons in extrastriate visual cortex with direct feedback connections to the LGN. Additionally, given that previous studies have demonstrated parallel streams of corticogeniculate feedback from V1 and V2 to the LGN (Briggs et al. 2016; Briggs and Usrey 2009; Hasse et al. 2019), we also asked whether there is morphological evidence for parallel streams of corticogeniculate feedback originating in extrastriate visual cortex.

A hallmark of visual systems in highly visual animals, such as primates and carnivores, is parallel processing of visual information through distinct feedforward streams that begin

in the retina and continue through the LGN into V1 (Callaway 2005; Kaplan 2004; Sherman and Guillery 2006). In primates, parvocellular, magnocellular and koniocellular streams are the foundation for acuity, motion, and color perception (Kaplan 2004). The X, Y and W streams in carnivores are somewhat, but not strictly, homologous to the primate parvocellular, magnocellular, and koniocellular streams (Sherman and Guillery 2006). For convenience, we refer to these pathways as “parvocellular/X”, etc., but acknowledge the lack of strict homology across species. There is strong evidence to suggest that corticogeniculate feedback circuits are organized into parallel streams that align with the feedforward parallel streams (Hasse and Briggs 2017b). Previous studies characterizing the physiology of corticogeniculate neurons revealed the presence of Simple and Complex corticogeniculate cell types with differing axon conduction speeds (Briggs & Usrey 2005, 2007; Grieve & Sillito 1995; Harvey 1978; Tsumoto & Suda 1980). In primates, Simple and Complex corticogeniculate neurons with different axon conduction speeds also displayed physiologically distinct response properties aligned with magnocellular, parvocellular, and koniocellular LGN neuronal responses (Briggs and Usrey 2009). Additionally, corticogeniculate neurons in V1 and V2 of both primates and carnivores displayed striking morphological diversity (Briggs et al. 2016; Gilbert and Kelly 1975; Hasse et al. 2019; Ichida et al. 2014; Katz 1987). Unique corticogeniculate cell types included short and tall cells, defined by apical dendrites limited to layer 4 versus extending into layer 2/3, and cell bodies located in the upper and lower tiers of layer 6, respectively (Briggs et al. 2016; Gilbert and Kelly 1975; Hasse et al. 2019; Katz 1987). Notably, the upper and lower tiers of layer 6 receive direct parvocellular and magnocellular inputs via geniculocortical axon collaterals (Blasdel and Lund 1983; Hendrickson et al. 1978). Additionally, corticogeniculate neurons in the upper and lower tiers of layer 6 project to the parvocellular and magnocellular LGN layers, respectively (Fitzpatrick et al. 1994). Together, these findings suggest that short corticogeniculate neurons belong to the parvocellular/X stream while tall corticogeniculate neurons belong to the magnocellular/Y stream (Hasse and Briggs 2017b). Following similar logic, less numerous and more unusual corticogeniculate cell types, including tilted, tall-tufted or large, and stellate cells, may belong to the koniocellular/W stream (Briggs et al. 2016; Hasse et al. 2019).

While the majority of geniculocortical and corticogeniculate circuits link the LGN with V1 (Hendrickson et al. 1978; Humphrey et al. 1985a, b), a smaller population of corticogeniculate neurons are located in V2 (Briggs et al. 2016; Hasse et al. 2019; Lin and Kaas 1977). The existence of corticogeniculate neurons in V2 further suggests that there may also be corticogeniculate neurons in other extrastriate visual areas. Briggs et al. (2016) and Hasse et al. (2019) reported observing corticogeniculate neurons in extrastriate visual areas beyond V2/area 18 even though they did not attempt to characterize them. In this study, we searched for corticogeniculate neurons specifically in three ferret mid-level extrastriate visual areas: the posteromedial lateral suprasylvian (PMLS, sometimes referred to as posterior suprasylvian area or PSS), the posterolateral lateral suprasylvian (PLLS) and area 21a. The ferret visual system shares striking similarities with the visual systems of other carnivores, like cats, and primates (Jackson and Hickey 1985). Ferrets have a relatively large visual system, with 19 separate anatomically defined areas (Homman-Ludiyé et al. 2010), including multiple areas with possible homology to primate extrastriate visual

areas. Like primate MT, ferret PMLS has highly direction selective neurons (Philipp et al. 2006) that receive input from V1 neurons biased towards motion processing (Jarosiewicz et al. 2012). Additionally, SMI-32 staining reveals large, darkly labeled neurons in PMLS, suggesting that this area receives strong Y pathway input (Homman-Ludiye et al. 2010). PMLS neurons also respond to complex motion stimuli (Lempel and Nielsen 2019) and PMLS lesions cause behavioral deficits in motion detection tasks (Hupfeld et al. 2007), all of which support its proposed homology with MT. Ferret area PLLS shares some similarities with cat area PLLS and its primate homolog the medial superior temporal area or MST (Li et al. 2000). SMI-32 staining in PLLS revealed the presence of large, darkly labeled neurons (Homman-Ludiye et al. 2010), suggesting that PLLS also receives strong Y-pathway input, consistent with its role in motion processing (Grant and Hilgetag 2005; Li et al. 2000). Ferret area 21a is homologous to cat area 21a and primate area V4 (Homman-Ludiye et al. 2010). Given these homologies, the presence of corticogeniculate neurons in PMLS, PLLS, and 21a would provide compelling evidence in favor of feedback circuits complementary to direct geniculocortical connections between the LGN and mid-level extrastriate visual cortical areas.

If present, corticogeniculate neurons in mid-level extrastriate areas may also be organized into parallel streams, since current evidence supports multiple morphologically distinct corticogeniculate cell types within a given visual cortical area (Briggs et al. 2016; Gilbert and Kelly 1975; Hasse et al. 2019; Ichida et al. 2014; Katz 1987). Following this idea, there may be different proportions of corticogeniculate cell types in areas PMLS, PLLS, and 21a because each of these areas is uniquely functionally specialized. Specifically, area 21a may have a larger proportion of short corticogeniculate cells with stronger ties to the X stream. Areas PMLS and PLLS may have a larger proportion of tall corticogeniculate cells with stronger ties to the Y stream. Alternatively, corticogeniculate neurons in mid-level extrastriate visual areas could be more morphologically and physiologically homogeneous with functional connections to a single stream, i.e., the koniocellular/W stream. This latter idea is supported by the fact that geniculocortical neurons with direct connections to MT and PMLS appear to be located mainly within the koniocellular and C layers of the LGN, and persistent MT activity following V1 cooling is sensitive to S-cone stimuli (Jayakumar et al. 2013; Sincich et al. 2004; Tong et al. 1982). In this scenario, corticogeniculate neurons in PMLS, PLLS, and 21a are likely to be the more unusual cell types observed previously, including tall-tufted or large, tilted, and stellate cells. Furthermore, these unusual cell types may or may not be similarly distributed across the three areas.

To determine the presence and morphological diversity of corticogeniculate neurons in mid-level extrastriate visual areas, we reconstructed the full dendritic morphology of virus-labeled corticogeniculate neurons in areas PMLS, PLLS and 21a from histological tissue collected as a part of a previous study (Hasse and Briggs 2017a). We utilized clustering algorithms to rigorously classify extrastriate corticogeniculate neurons and to determine whether corticogeniculate neurons within and across the three areas were morphologically heterogeneous or diverse. These analyses revealed the presence of corticogeniculate cell types similar to those observed previously as well as new corticogeniculate types with morphological features intermediate to those of standard short and tall cells. Interestingly, distributions of corticogeniculate cell types across PMLS, PLLS, and 21a were not similar,

with cells from a single area often dominating individual morphologically defined clusters. Together, these findings suggest that V1-independent connectivity between the LGN and extrastriate visual cortex involves complementary direct feedforward geniculocortical and feedback corticogeniculate connections. Although each mid-level extrastriate area contained morphologically diverse corticogeniculate cell types, different proportions of unique cell types per area suggests a unique parallel organization for corticogeniculate feedback from extrastriate visual cortex to the LGN.

Methods and materials

All of the tissue examined for this study was prepared as a part of a previous study (Hasse and Briggs 2017a). All the experimental methods involving animals have been described in detail in the Materials and Methods and SI Appendix: Materials and Methods of Hasse and Briggs (2017a) and were approved by the Institutional Animal Care and Use Committee at Dartmouth. Descriptions of the methods for stereotaxic injection of SAD-B19 rabies virus into the dorsal lateral geniculate nucleus (LGN), harvesting of brain tissue, sectioning, staining, and reconstruction of virus-labeled neurons have also been described in detail previously (Bragg and Briggs 2017; Bragg et al. 2017; Briggs et al. 2016; Hasse et al. 2019).

For this study, data were analyzed from seven adult female ferrets (*Mustela putorius furo*). In all seven ferrets, a genetically modified rabies virus, SAD G-ChR2-mCherry (Osakada et al. 2011; Wickersham et al. 2007), was injected into the LGN to drive expression of channelrhodopsin2 and mCherry in corticogeniculate neurons via retrograde infection (Hasse et al. 2019; Hasse and Briggs 2017a). Importantly, because the modified rabies virus lacked the ability to cross synapses and exclusively infected neurons in a retrograde manner, the only neurons in the visual cortex to express the fluorescent marker mCherry were corticogeniculate neurons. Also, because virus-mediated expression of mCherry caused widespread labeling of individual neurons, it was possible to reconstruct large numbers of corticogeniculate neurons spanning multiple mid-level extrastriate visual areas including areas within the posterior suprasylvian area: posteromedial lateral suprasylvian area (PMLS) and posterolateral lateral suprasylvian area (PLLS), as well as extrastriate visual area 21a. Finally, because mCherry was expressed throughout the dendritic arbors of infected corticogeniculate neurons (Fig. 1), we were able to reconstruct and quantify the morphological diversity of a large sample of corticogeniculate neurons and apply rigorous statistical methods to classify distinct morphological subtypes within and across these extrastriate visual areas.

All experimental details have been described previously (Hasse and Briggs 2017a) but are briefly summarized below. In a sterile surgical procedure utilizing aseptic techniques, a small craniotomy was made over the LGN and small volumes (~ 5 μ l) of rabies virus injected into the LGN under stereotaxic and neurophysiological guidance using a nano-liter injector (Nanoject II: Drumond Scientific, Broomall, PA). Animals recovered for about 1 week following surgery and then underwent a non-recovery acute neurophysiological recording procedure, the endpoint of which was euthanasia, perfusion, and harvesting of brain tissue. The visual cortex was sectioned coronally at a thickness of 70 μ m using a freezing microtome. Sections were stained for cytochrome oxidase activity and

using antibodies against mCherry (rabbit anti-DS red, polyclonal, Clontech Laboratories Inc., Mountain View, CA, RRID: AB_10013483) followed by a biotinylated secondary antibody (goat anti-rabbit, Molecular Probes/Life Technologies, Grand Island, NY). Tissue was reacted with DAB and peroxide to permanently stain corticogeniculate neurons, then sections were mounted on glass slides, dehydrated, defatted, and cover-slipped.

First, we verified that virus injections in all seven ferrets were restricted to the LGN: Supplemental Fig. 1 of Hasse and Briggs (2017a) illustrates example coronal LGN sections and 3-D reconstructed injection site volumes within the LGN for all seven of the ferrets studied here. Volumes of virus injections for six ferrets ranged from 5–22% of total LGN volume. In one ferret, the injection volume was 43%. Retinotopic regions covered by virus injection volumes included every part of the LGN across ferrets, although in the majority of ferrets (5 of 7), injection volumes included or were close to the area centralis representation of the LGN. Retinotopic extents of virus injections corresponded to at least 20 degrees of visual space in the majority of ferrets. Next, we counted the number of labeled corticogeniculate neurons in PMLS, PLLS, and area 21a in each ferret and verified that these were located within layer 6, as prior studies have shown that corticogeniculate neurons observed in V1 and V2 of primates and areas 17 and 18 of carnivores are restricted to layer 6 (Briggs et al. 2016; Fitzpatrick et al. 1994; Gilbert and Kelly 1975; Hasse et al. 2019; Ichida et al. 2014; Katz 1987; Lin and Kaas 1977; Lund et al. 1975; Usrey and Fitzpatrick 1996). We counted a total of 230 corticogeniculate neurons in PMLS, PLLS, and area 21a across seven ferrets. As we did not necessarily have equal numbers of sections containing each extrastriate visual area per ferret, we normalized the number of corticogeniculate neurons counted within each area by the number of sections containing each area per ferret (Fig. 1c). Importantly, all sections examined contained at least one virus labeled corticogeniculate neuron. Of the 230 total corticogeniculate neurons in PMLS, PLLS and area 21a, 7 labeled corticogeniculate appeared to be displaced outside of layer 6 (3 each in PMLS and PLLS, 1 in area 21a). In all seven of these cases, the layers were difficult to discern due to the plane of section relative to the curvature of the cortex. It is therefore likely that many, if not all, of these seven apparently displaced corticogeniculate neurons were actually within layer 6. We did not reconstruct these seven possibly displaced corticogeniculate neurons.

To reconstruct the full dendritic morphology of corticogeniculate neurons in areas PMLS, PLLS, and 21a, we first selected neurons that were separated from neighboring neurons, i.e., outside of clusters of labeled corticogeniculate neurons, and that were well labeled. We reconstructed a total of 20 corticogeniculate neurons in PMLS, 20 corticogeniculate neurons in PLLS, and 10 corticogeniculate neurons in area 21a (range = 1–7 PMLS neurons per ferret, mean = 3.3 PMLS neurons per ferret; range = 2–6 PLLS neurons per ferret, mean = 3.33 PLLS neurons per ferret; range = 1–4 area 21a neurons per ferret, mean = 2 area 21a neurons per ferret). A NeuroLucida system (MicroBrightField, Williston, VT) with an Optronics camera attached to an Olympus Provis microscope (Olympus Corporation, Center Valley, PA) was used to trace the contours and boundaries of PMLS, PLLS, and area 21 within each section, to mark and count labeled corticogeniculate neurons per area, to draw laminar boundaries around each reconstructed neuron based on the cytochrome oxidase stain, and to trace the outlines of the cell bodies and dendritic arbors. We only reconstructed neurons with cell bodies entirely contained within a single home section to accurately

estimate the cell body area and roundness. Basal and apical dendritic arbors originating from the cell body were traced, placing nodes at each branch point and endings at each branch termination. Dendritic arbors were traced through three adjacent sections for all neurons, including the home section containing the cell body and one section above and one below the home section. For three corticogeniculate neurons, it was possible to trace axonal arbors as well, but these were not further quantified as it was usually not possible to trace axons for the majority of labeled corticogeniculate neurons.

Rigorous clustering algorithms, principal components analysis (PCA), and statistical methods were used to quantify morphological differences across reconstructed corticogeniculate neurons as described previously (Bragg and Briggs 2017; Bragg et al. 2017; Briggs et al. 2016; Hasse et al. 2019). First, the following morphological metrics were quantified and extracted per reconstructed corticogeniculate neuron. Cell body area was computed as the area of the cell body contour, drawn through the largest extent of the cell body within the home section. Cell body roundness was computed from the cell body contour. The number of nodes and endings was extracted per reconstructed neuron. Cell body position within layer 6 was measured as the proportional distance between the cell body and the contour marking the top of layer 6 compared to the full extent of layer 6 (measured as the distance between the top of layer 6 and the layer 6/white matter border). The height of the apical dendrite was measured as the proportional distance between the top of the apical dendrite and the top of layer 2/3 compared to the full cortical depth (measured as the distance between the top of layer 2/3 and the layer 6/white matter border). For stellate neurons that lacked an apical dendrite, the top of the dendrite closest to the top of layer 2/3 was used for an analogous measurement. Percentages of basal dendrite in layers 4, 5, 6, and in the white matter were computed by dividing the basal dendrite per layer by the total length of basal dendrite per neuron and converting proportion to percentage. Percentages of apical dendrite in layers 2/3, 4, 5, 6, and above layer 2/3 were computed by dividing the apical dendrite per layer by the total length of apical dendrite per neuron and converting proportion to percentage.

We first performed a cluster analysis to define morphologically distinct clusters of corticogeniculate neurons. We included all 50 reconstructed neurons and we did not include any information about the area of origin of each reconstructed corticogeniculate neuron in the cluster analysis. We included a total of 14 independent morphological metrics in the cluster analysis: cell body area, cell body roundness, number of nodes, percentage of basal dendrite in layers 4, 5, 6, and the white matter, percentage of apical dendrite in layers 2/3, 4, 5, 6, and above layer 2/3, cell body position in layer 6, and apical dendrite height or tallest point on stellate neurons (see Tables 1, 2 and 3). The only metric excluded from the cluster analysis was the number of endings, because this is not independent of the number of nodes and the cluster algorithm assumes each parameter is independent and gives each metric equal weight (Bragg et al. 2017; Cauli et al. 2000; Thorndike 1953). For the cluster analysis, the Euclidean distance between each neuron, defined by a point in a 14-dimensional space, was computed using the 'pdist' function in Matlab (Mathworks Inc., Natick, MA). Clusters were defined by the inner squared distance between neurons using the 'linkage' function and applying Ward's method. The 'dendrogram' function was used to visualize the linkage distances between neurons and to illustrate clusters (Fig. 2a).

To statistically verify the optimal number of clusters of distinct extrastriate corticogeniculate neuronal types, we performed two independent tests. First, we tested for the optimal cluster number between 1 and 6 possible clusters using the ‘evalclusters’ function which employs the Calinski/Harabasz method to evaluate optimal cluster number based on a set of defined criteria (Calinski and Harabasz 1974). As a second test that was independent of the cluster analysis, we used a Gaussian mixture model (GMM) clustering algorithm (Talebi and Baker 2016). We performed PCA on the same 14 morphological metrics used in the cluster analysis (Fig. 2b) and applied the PCA scores to test GMMs, again assuming 1 to 6 possible clusters (using the ‘fitgmdist’ function). Three different GMM evaluations were used: negative log likelihood, Akaike information criterion, and Bayes information criterion. The GMM with the lowest criteria across the three evaluations indicated the optimal number of clusters.

Once the optimal cluster number was determined using the statistical evaluations described above, we grouped all of the reconstructed corticogeniculate neurons according to their cluster assignment. We then counted the number of corticogeniculate neurons originating in each extrastriate area per cluster. We performed statistical tests of each morphological metric across neurons per cluster using non-parametric multiple-comparisons tests (Kruskal Wallis oneway ANOVA) and corrected all final p values for multiple comparisons using Bonferroni correction. Averages and standard error on the mean (SEM) are reported per metric per cluster along with p values for each metric comparison across clusters in Tables 1, 2 and 3.

Results

Whether direct feedforward geniculocortical connections from the LGN to extrastriate visual cortex are complemented by reciprocal feedback corticogeniculate connections and whether these connections represent distinct functional streams are not known. To address these questions, we examined histological tissue collected as a part of a previous study (Hasse and Briggs 2017a) in which a modified rabies virus was injected into the LGN of ferrets to selectively retrogradely label corticogeniculate neurons (Briggs et al. 2016; Hasse et al. 2019; Hasse and Briggs 2017a). We focused our analyses on three mid-level extrastriate visual areas: posteromedial lateral suprasylvian area (PMLS), posterolateral lateral suprasylvian area (PLLS), and area 21a due to their proposed homology with primate areas MT, MST, and V4 (Homman-Ludiye et al. 2010; Hupfeld et al. 2007; Lempel and Nielsen 2019; Philipp et al. 2006). All three ferret extrastriate visual areas examined contained sparse, but consistently present virus-labeled corticogeniculate neurons that were mainly restricted to layer 6 (Fig. 1a, b). There were clear differences in the density of virus-labeled corticogeniculate neurons between areas 17 and 18 and areas 21a, PMLS, and PLLS (e.g., Fig. 1b). In 7 ferrets, we observed a total of 230 virus-labeled extrastriate corticogeniculate neurons: 35 in PMLS, 59 in PLLS, and 136 in 21a (Fig. 1c). PMLS and PLLS are smaller than 21a (Radtke-Schuller 2018) and we had more sections containing 21a (35 sections across 7 ferrets) compared to PMLS (17 sections across 6 ferrets) and PLLS (18 sections across 6 ferrets). This may explain the larger number of virus-labeled corticogeniculate neurons counted in 21a. However, given the limitations of available sections and differences in the size of each area, we postulate there are roughly equivalent densities of virus-labeled corticogeniculate neurons in PMLS, PLLS, and 21a

(Fig. 1c). Out of 230 virus-labeled corticogeniculate neurons, 7 could not be verified to be located within layer 6 due to the plane of section relative to the curvature of the cortex. All other labeled corticogeniculate neurons were unambiguously located within layer 6, consistent with observations of corticogeniculate neurons in areas 17/V1 and 18/V2 (Briggs et al. 2016; Fitzpatrick et al. 1994; Gilbert and Kelly 1975; Ichida et al. 2014; Katz 1987; Lin and Kaas 1977).

We observed notable differences in dendritic morphology across extrastriate corticogeniculate neurons in areas PMLS, PLLS, and 21a (Fig. 1d–g). Figure 1g illustrates representative reconstructions of the full dendritic arborizations of nine extrastriate corticogeniculate neurons distributed across the three areas under study. These included corticogeniculate morphological types described previously (Hasse & Briggs 2017b): spiny stellate corticogeniculate neurons (Fig. 1g, yellow), tall corticogeniculate neurons with superficial branches and tufts in and above layer 2/3 (Fig. 1g, dark green), tall corticogeniculate neurons without superficial tufts (Fig. 1g, red), short corticogeniculate neurons with standard short characteristics like apical dendritic branches in layer 4 (Fig. 1g, cyan), and more unusual short corticogeniculate neurons including those with tilted apical dendrites (Fig. 1g, orange). In addition to morphological types observed previously, we also noted extrastriate corticogeniculate neurons that were somewhat intermediate to standard tall and short corticogeniculate neurons (Fig. 1g, light green). To rigorously determine whether extrastriate corticogeniculate neurons in the 3 areas were morphologically heterogeneous, we performed a cluster analysis on 50 reconstructed extrastriate corticogeniculate neurons (20 each in PMLS and PLLS and 10 in 21a) using 14 morphological metrics (listed in Tables 1, 2 and 3 and see Methods and Materials). Importantly, there was no information about the extrastriate area of origin for any corticogeniculate neuron in the cluster analysis. The cluster analysis independently weighted each morphological metric and plotted the distance between neurons in a 14-dimensional space, then clustered neurons based on least-squared distances between groups of neurons in that space. Figure 2a illustrates the dendrogram of linkage distances between each neuron. We performed two independent statistical tests to determine the optimal number of clusters from this analysis. Application of the Calinski/Harabasz method and a Gaussian mixture model to evaluate optimal cluster number both gave optimal cluster numbers of 6. This evaluation of six unique clusters was consistent even when up to 2 metrics were removed from the cluster analysis, suggesting that the six clusters of morphologically distinct extrastriate corticogeniculate neurons were robustly defined. In addition to the cluster analysis, we also performed PCA on the same 14 morphological metrics and the representations of the first two principal components were nicely separated when color-coded by the cluster assignment obtained from the cluster analysis (Fig. 2b). Thus, through multiple independent methods, we quantitatively classified extrastriate corticogeniculate neurons in areas PMLS, PLLS, and 21a into six morphologically distinct groups.

Quite surprisingly, corticogeniculate neurons from each of the three extrastriate areas were not evenly distributed across the six clusters (Fig. 2a, colored bars indicate area of origin of each neuron, which was not a variable included in the cluster analysis). Cluster 1 was heavily dominated by PMLS neurons (8 of 12 neurons), Clusters 2, 3, and 5 were dominated by PLLS neurons (6 of 9, 4 of 7, and 4 of 6 neurons, respectively), and Cluster 4 was

dominated by 21a neurons (5 of 10 neurons). Cluster 6 also had more PMLS than PLLS or 21a neurons, although there were fewer total neurons in this cluster. While most clusters contained neurons originating in all three areas (except Clusters 3 and 5, which both lacked 21a neurons), corticogeniculate neurons of each type were not evenly distributed across these extrastriate areas. Combination of qualitative morphological classifications with results of the cluster analysis (e.g., compare Figs. 1g and 2a) suggested the following uneven distributions of corticogeniculate types across extrastriate areas. PMLS contained mostly stellate and short corticogeniculate neurons with unusual features like tilted apical dendrites (11 of 20 PMLS neurons in Clusters 1 and 6). PLLS corticogeniculate neurons were mostly tall branched/tufted, standard short, or in between with medium-tall (termed “intermediate”) apical dendrites (14 of 20 PLLS neurons in Clusters 2, 3, and 5). Corticogeniculate neurons in 21a mostly had standard tall morphology (5 of 10 21a neurons in Cluster 4). It is important to note that PMLS is within the suprasylvian sulcus and mainly restricted to the cortical region with a significant bend that compresses the cortical layers (Fig. 1a, d). This cortical architecture may influence apical dendrite height among PMLS corticogeniculate neurons.

Given the uneven distribution of the unique types of extrastriate corticogeniculate neurons across areas, we next explored the morphological features that most defined corticogeniculate neurons in each cluster (Fig. 3 and Tables 1, 2 and 3). Cluster 1 neurons were unique in that they had fewer nodes (i.e., fewer total dendritic branches; Fig. 3b), their dendrites rarely extended above the layer 5/6 border (Fig. 3d), and their apical and basal dendrites were mostly restricted to layer 6 (Fig. 3e, h), rarely extending into layer 5 (Fig. 3f, i) and never into layer 4 (Fig. 3g, j). Indeed, Cluster 1 neurons differed significantly from neurons in other clusters based on many of these attributes including number of nodes, overall dendrite height, and percentage of apical dendrite in layers 6 and 4 (Tables 1 and 2). These characteristics are consistent with the majority of Cluster 1 corticogeniculate neurons being spiny stellate neurons and/or neurons with very little apical dendrite (Fig. 1g). Neurons in Cluster 2 had the smallest cell bodies (Fig. 3a) and the tallest apical dendrites (Fig. 3d) among all the clusters. Notably, Cluster 2 neurons had basal dendrites almost entirely restricted to layer 6 (Fig. 3e–g), but more apical dendrites in layer 2/3 than any other cluster (Fig. 3k; Table 2) and more apical dendrites above layer 2/3 than most other clusters (Table 2). These traits are consistent with tall tufted corticogeniculate neurons observed in area 18 of ferrets (Hasse et al. 2019). Neurons in Cluster 3 were unique in that they had significantly larger cell bodies compared to neurons in all other clusters (Fig. 3a, Table 1). Cluster 3 neuronal cell bodies were often located closer to the layer 5/6 border (Fig. 3c). The tallest point on the apical dendrite of Cluster 3 neurons was intermediate to that of neurons in the other clusters (Fig. 3d), consistent with the fact that their apical dendrites were mostly evenly distributed across layers 6, 5, and 4, with some apical dendrite in layer 2/3 (Fig. 3h–k; Table 2). Also, Cluster 3 neurons had more basal dendrite in layer 4 than any other cluster (Fig. 3g; Table 3). Together, these features define Cluster 3 corticogeniculate neurons as a new type of large-cell body neurons that are intermediate to the standard short and tall corticogeniculate neurons described previously. Neurons in Cluster 4 were somewhat similar to those in Cluster 2 with relatively small cell bodies (Fig. 3a; Table 1) and tall apical dendrites (Fig. 3d; Table 2). Cluster 4 neurons differed from Cluster 2

neurons in that they had more basal dendrite in layer 4 (Fig. 3g; Table 3) and less apical dendrite in layer 2/3 (Fig. 3k; Table 2). Neurons in Cluster 5 had medium sized cell bodies (Fig. 3a) and although some had taller apical dendrites (Fig. 3d), the majority of their apical dendrites were in layers 5 and 4 (Fig. 3i–j; Table 2), consistent with standard short corticogeniculate morphology. Cluster 5 neurons also had more basal dendrites in layer 5 compared to the other clusters (Fig. 3f; Table 3). Neurons in Cluster 6 had medium sized cell bodies (Fig. 3a) that were usually located relatively deep in layer 6 toward the white matter (Fig. 3c) and short apical dendrites (Fig. 3d; Table 2). Accordingly, the majority of the apical dendrites of Cluster 6 neurons were in layer 6 with smaller amounts in layer 5 and 4 and little in layer 2/3 (Fig. 3h–k; Table 2). Likewise, the basal dendrites of Cluster 6 neurons were largely restricted to layer 6 (Fig. 3e–g; Table 3). All of these features are similar to tilted corticogeniculate neurons described previously (Briggs et al. 2016; Hasse et al. 2019). Indeed, the apical dendrites of many Cluster 6 neurons appeared to exit the cell body at the side and were tilted relative to the cortical layers (Fig. 1g, orange reconstructions).

Although corticogeniculate neurons in the six clusters differed across most of the morphological metrics included in the cluster analysis, for some of the metrics, corticogeniculate neurons were broadly similar. Corticogeniculate neurons had similarly round cell bodies, quantified by a roundness value (Table 1). As expected for neurons in layer 6, all corticogeniculate neurons had the majority of their basal dendrites in layer 6 (Fig. 3e, Table 3). Only Cluster 5 neurons had a more substantial percentage (~ 22%) of basal dendrites in layer 5 and neurons in just three clusters had greater than 1% of basal dendrites in layer 4 (Fig. 3f, g; Table 3). Also consistent with their cell body location in layer 6, few corticogeniculate neurons had apical dendrites that extended above layer 2/3: only the tall and tall-tufted cells in Clusters 2 and 4 had greater than 1% of apical dendrites above layer 2/3 (Table 2). Thus, although corticogeniculate cell types were clearly differentiated across a number of morphological dimensions, they were similar with regard to properties expected among deep layer cortical neurons. Taken together, quantifications of the various morphological metrics across neurons in the six clusters supported qualitative characterizations of extrastriate corticogeniculate neurons into previously described types and also identified a novel type of corticogeniculate neuron (Cluster 3 neurons) with large cell bodies and intermediate morphology relative to short and tall corticogeniculate neurons described previously.

Discussion

The first major feedback circuit in the visual system is made up of corticogeniculate neurons that reside in the visual cortex and project axons to the LGN. Corticogeniculate feedback likely plays a critical role in vision by complementing feedforward geniculocortical circuits that convey visual information from the retina to the visual cortex. When V1 is damaged, some residual vision remains, a phenomenon known as blindsight (Weiskrantz 2009). Blindsight is thought to be mediated at least in part by direct geniculocortical connections to extrastriate visual cortex that bypass V1 (Dell et al. 2018; Lyon and Rabideau 2012; Lysakowski et al. 1988; Sherk 1986; Sincich et al. 2004; Tong et al. 1982). If complementary reciprocal feedforward and feedback connections are critical for vision, including in blindsight, we reasoned that direct geniculocortical connections to extrastriate

areas are complemented by corticogeniculate feedback originating in extrastriate cortex. Furthermore, anatomical and physiological evidence from primates and carnivores suggests that corticogeniculate circuits are comprised of multiple distinct cell types that carry stream-specific information from the visual cortex to the LGN (Briggs and Usrey 2005, 2007, 2009; Conley and Raczkowski 1990; Fitzpatrick et al. 1994; Grieve and Sillito 1995; Harvey 1978; Hasse et al. 2019; Ichida et al. 2014; Katz 1987; Lund and Boothe 1975; Tsumoto and Suda 1980; Usrey and Fitzpatrick 1996). We therefore sought to determine whether corticogeniculate neurons exist in mid-level extrastriate visual cortex and whether they are morphologically homogeneous or diverse, to learn more about possible parallel streams of direct, reciprocal connectivity between the LGN and extrastriate visual cortex.

We have previously used G-deleted rabies virus to drive the expression of fluorescent proteins selectively in corticogeniculate neurons and examined the morphological diversity of these cells in area 17/V1 and area 18/V2 of ferrets and macaque monkeys (Briggs et al. 2016; Hasse et al. 2019). Morphometric analysis of virus-labeled corticogeniculate neurons in area 17/V1 and area 18/V2 revealed the presence of morphologically distinct cell types with dendritic and axonal arborization patterns supporting their involvement in stream-specific processing of visual information. In this study, we reconstructed the complete dendritic morphology of virus-labeled corticogeniculate neurons in three mid-level extrastriate visual areas in ferrets, PMLS, PLLS and 21a. Corticogeniculate neurons were present in areas PMLS, PLLS, and 21a (Fig. 1), confirming our prediction that direct geniculocortical inputs to extrastriate visual areas are complemented by reciprocal corticogeniculate circuits. Interestingly, independent cluster analyses of corticogeniculate morphology revealed different distributions of distinct corticogeniculate cell types in each of the three extrastriate areas (Fig. 2). Although the same corticogeniculate cell types observed previously in area 17/V1 and area 18/V2 were also present in ferret extrastriate cortex, a novel corticogeniculate cell type with dendritic arborization patterns intermediate to tall and short corticogeniculate neurons was also observed, mainly in PLLS (Figs. 1, 2 and 3). Our discovery of corticogeniculate neurons in mid-level extrastriate visual cortex suggests that residual vision in blindsight may be mediated in part by complementary reciprocal connections between the LGN and extrastriate visual areas that are independent of V1. The presence of multiple distinct corticogeniculate cell types in PMLS, PLLS, and 21a suggests a parallel organization of corticogeniculate feedback within each area. However, different proportions of corticogeniculate cell types across PMLS, PLLS, and 21a also suggest some functional specialization of these parallel feedback pathways.

We are confident that the virus-labeled neurons we observed in PMLS, PLLS, and 21a are corticogeniculate neurons and not corticopulvinar neurons or other subcortically projecting neurons. All but seven virus-labeled neurons were unambiguously located within layer 6. This suggests that virus injections did not encroach into the ventral LGN, lateral posterior nucleus, or the thalamic reticular nucleus at the anterior edge of the LGN, because these structures receive inputs from layer 5 corticothalamic neurons (Conley and Friederich-Ecsy 1993; Fitzgibbon et al. 1999; Jones 2002; Lund et al. 1975; Rockland 1994) and we did not observe virus-labeled neurons in layer 5. Close scrutiny of virus injection zones in each of the cases utilized in this study revealed that in one ferret, some virus may have encroached into the geniculocortical and/or the anterior thalamic reticular nucleus. However, virus injected

into the perigeniculate would have labeled corticogeniculate neurons via axon collaterals (Sherman and Guillery 2006). Additionally, virus-labeled neurons were not observed above layer 6 in this ferret.

Although we observed virus-labeled corticogeniculate neurons in PMLS, PLLS, and 21a following retrograde virus injections into the LGN, the density of corticogeniculate neurons in mid-level extrastriate cortical areas was significantly lower than that previously reported for areas 17 and 18 (e.g., Fig. 1b). This observation is consistent with densities of corticogeniculate neurons observed across visual areas in cats. Specifically, corticogeniculate neurons make up approximately 50% of layer 6 neurons in cat area 17 (Gilbert and Kelly 1975; Katz 1987) and a smaller proportion of layer 6 neurons in areas 18 and 19, with corticogeniculate neurons observed beyond area 19 reported as “sparse” (Gilbert and Kelly 1975). We observed 230 virus-labeled extrastriate corticogeniculate neurons in 7 ferrets. In comparison, Hasse et al. (2019) observed thousands of virus-labeled corticogeniculate neurons in areas 17 and 18 from an overlapping cohort of six ferrets. Qualitative assessment of the Hasse et al. (2019) dataset also suggests that area 17 likely contained almost one order of magnitude greater virus-labeled corticogeniculate neurons compared to area 18. Our qualitative assessment of the cohort of ferrets used in this study and those used by Hasse et al. (2019) also suggests that area 18 contains almost one order of magnitude greater virus-labeled corticogeniculate neurons compared to PMLS, PLLS, and 21a combined. Overall, our qualitative estimates suggest that the proportion of corticogeniculate neurons decreases by almost an order of magnitude at each processing stage from area 17 to area 18 to mid-level extrastriate visual cortical areas, consistent with qualitative estimates reported previously (Gilbert and Kelly 1975). Within the mid-level extrastriate cortical areas examined here, the numbers of virus-labeled corticogeniculate neurons appeared to vary, with a larger cell count in area 21a compared to PMLS and PLLS. However, a qualitative assessment of the relative density of virus-labeled corticogeniculate neurons per area. The difference in total virus-labeled cell counts across mid-level areas is likely due to the fact that area 21a is larger than PMLS and PLLS (Radtke-Schuller 2018). Our sample of tissue sections included twice as many sections containing area 21a compared to sections containing PMLS or PLLS, which likely explains the larger number of virus-labeled corticogeniculate neurons observed in 21a (Fig. 1). Our use of a highly sensitive retrograde tracing method (virus-mediated gene expression) revealed not only the robust corticogeniculate connections from areas 17 and 18 to the LGN, but also sparser corticogeniculate connections from mid-level extrastriate visual cortex. It is important to note, however, that although extrastriate corticogeniculate neurons are sparse, they could still exert a functional influence over the LGN. Gilbert and Kelly (1975) observed an increase in the size of cell bodies among extrastriate compared to area 17 corticogeniculate neurons. It is possible that these larger cells constitute unique groups of corticogeniculate neurons with distinct functional impacts upon LGN neurons.

Not only does the virus-mediated retrograde tracing technique reveal sparse connections, it also reveals rare and unusual cell types within the population because of its high efficacy. Using this method, we previously observed multiple morphologically distinct corticogeniculate neurons including the more common standard short and tall

corticogeniculate neurons, thought to be affiliated with the X/parvocellular and Y/magnocellular feedforward streams, respectively, as well as rarer and unusual spiny stellate, non-standard short or tilted, and tall-tufted cell types (Briggs et al. 2016; Hasse et al. 2019). In this study, our morphological analysis of dendritic arborization patterns among extrastriate corticogeniculate neurons revealed a similar diversity of corticogeniculate cell types across PMLS, PLLS, and 21a (Fig. 1). In addition to the cell types listed above, we also observed a new corticogeniculate cell type (Fig. 1g, light green) with intermediate morphology relative to standard short and tall corticogeniculate neurons. Notably, these intermediate corticogeniculate neurons were mostly confined to PLLS. In fact, the concentration of intermediate corticogeniculate cell types in PLLS is a good example of another remarkable finding: the diverse corticogeniculate cell types observed in mid-level extrastriate visual cortical areas were not equally distributed across the three areas. Critically, we omitted any reference to area of origin for extrastriate corticogeniculate neurons included in the independent cluster analysis. Surprisingly, the resulting six clusters defined by the clustering algorithm contained unequal distributions of neurons from PMLS, PLLS, and 21a (Fig. 2). Specifically, PMLS corticogeniculate neurons dominated Clusters 1 and 6; PLLS corticogeniculate neurons dominated Clusters 2, 3, and 5; and corticogeniculate neurons from 21a dominated Cluster 4. A closer look at the distribution of corticogeniculate cell types in each area revealed that PMLS contained mostly spiny stellate and non-standard short (e.g., tilted) corticogeniculate neurons (Fig. 2; Clusters 1 and 6). It is possible that shorter apical dendrites among PMLS corticogeniculate cell types were influenced by the compressed and curved shape of PMLS. PLLS mostly contained tall tufted, standard short, and the newly observed intermediate corticogeniculate neurons (Fig. 2; Clusters 2, 3, and 5). Area 21a contained mostly standard tall corticogeniculate neurons (Fig. 2; Cluster 4). Although it is possible that our criteria for reconstructing corticogeniculate neurons that were somewhat separated from other virus-labeled neurons may have biased us toward particular corticogeniculate types, we believe our reconstructions are representative of the relative proportions of observed cell types per area. Thus, although we observed diverse corticogeniculate cell types across three mid-level extrastriate visual areas, the distributions of each unique cell type were not equal in each of these areas. This unequal distribution raises the possibility that corticogeniculate feedback circuits originating in PMLS, PLLS and 21a convey functionally unique information directly to the LGN.

Surprisingly, the dominant corticogeniculate morphological cell types within each extrastriate area were not those predicted based on areal specialization. Although homology between 21a and V4 would suggest that corticogeniculate neurons in 21a should be aligned with the X/parvocellular stream (e.g., standard short cells), corticogeniculate cell types in 21a were mostly tall cells, consistent with links to the Y/magnocellular stream. Interestingly, 21a neurons retained most of their tuning when Y retinogeniculate activity was suppressed (Dreher et al. 1993), while corticocortical feedback from 21a to area 17 mainly modulated gain rather than tuning responses among area 17 neurons (Wang et al. 2000). Together, these results suggest complex relationships between the LGN, area 17, and area 21a that may involve multiple streams and multiple feedforward and feedback circuits. Even though homology between PMLS and MT would suggest that PMLS corticogeniculate neurons should be aligned with the Y/magnocellular stream (e.g., standard tall cells), we

observed more unusual corticogeniculate cell types in PMLS, suggesting links to the W/koniocellular stream. This finding is consistent with neuroanatomical studies showing that direct feedforward geniculocortical inputs to MT and PMLS originate from LGN cells in the koniocellular and C layers, respectively (Sincich et al. 2004; Tong et al. 1982). Also, Jayakumar et al. (2013) measured persistent S-cone modulatory responses in primate MT following V1 cooling, suggesting direct koniocellular pathway inputs to MT. If PMLS spiny stellate and non-standard/tilted corticogeniculate neurons synapse onto W LGN neurons and PMLS receives direct W pathway input, as in primates, this would be an elegant example of complementary reciprocal connectivity between the LGN W layers and extrastriate visual cortex. In contrast to PMLS and 21a, both of which were largely dominated by corticogeniculate cell types thought to be associated with a single stream, PLLS contained a greater variety of corticogeniculate cell types (standard short, tall tufted, and intermediate). Accordingly, PLLS corticogeniculate feedback could connect to LGN neurons in all three streams, X, Y, and W, respectively. Going forward, it will be interesting to determine whether there is direct, V1-bypassing geniculocortical input from X and Y LGN neurons to PLLS and 21a, providing complementary feedforward circuits to the feedback circuits observed. Additionally, comparative studies in primates to examine feedforward geniculocortical connectivity to areas MST and V4 would provide useful insight, especially given that X and Y geniculocortical neurons are intermixed in carnivore LGN (Humphrey et al. 1985a,b). Alternatively, extrastriate corticogeniculate morphology may not strictly align with or predict functional relationships with the feedforward parallel processing streams, but instead reflect additional factors that dictate functional specializations, such as alignment with functional modules defined by physiological properties like direction selectivity. Finally, it is important to note that caution is required when making functional predictions based purely on morphological data. Further studies linking physiological response properties with morphologically defined extrastriate corticogeniculate cell types will undoubtedly provide a clearer picture of the potentially unique contributions of corticogeniculate neurons originating in each extrastriate area.

Overall, our findings show that direct geniculocortical inputs to extrastriate visual areas are complemented by reciprocal corticogeniculate circuits. Furthermore, we observed a diversity of morphologically unique corticogeniculate cell types in mid-level extrastriate visual areas PMLS, PLLS, and 21a, providing a substrate for multiple stream-specific feedback projections to the LGN. In contrast to areas 17 and 18, both of which contained the full diversity of corticogeniculate cell types, PMLS, PLLS, and 21a contained unequal distributions of distinct corticogeniculate cell types. This finding in particular supports the notion that each of these mid-level extrastriate areas has a unique relationship with the LGN. Specifically, corticogeniculate feedback from PMLS and 21a may selectively target W and Y stream LGN neurons, while corticogeniculate feedback from PLLS may be more distributed across streams. Finally, our results show that at multiple visual processing stages along the visual cortical hierarchy, there are complementary feedforward and feedback circuits that link the LGN directly with each area. The presence of complementary circuits at all processing stages highlights the importance of both the feedforward and the feedback projections in supporting visual perception. Accordingly, it is likely that both feedforward

geniculocortical as well as complementary feedback corticogeniculate circuits are critical for maintaining residual vision following V1 damage, as in blindsight.

Acknowledgements

We thank Elise Bragg for expert technical assistance and Drs. Karen Moodie and Kirk Maurer for veterinary assistance. We thank Allison Murphy for helpful comments on the manuscript. Note: Invited submission to Brain Structure and Function special issue on “Structure and Function of the Visual System” edited by Drs. Takemura and Rosa.

Funding

This work was funded by National Institutes of Health (National Eye Institute: EY018683 and EY025219 to F.B.), National Science Foundation (EPSCoR 1632738), the Whitehall Foundation, the Hitchcock Foundation, the Del Monte Institute for Neuroscience at the University of Rochester, and a University of Rochester University Research Award. J.M.H. was supported by a Graduate Fellowship from the Albert J. Ryan Foundation.

Availability of data, material, and code

Data, material, and custom code that support the findings of this study are available from the corresponding author upon request.

References

- Azzopardi P, Fallah M, Gross CG, Rodman HR (2003) Response latencies of neurons in visual areas MT and MST of monkeys with striate cortex lesions. *Neuropsychologia* 41:1738–1756 [PubMed: 14527538]
- Blasdel GG, Lund JS (1983) Termination of afferent axons in macaque striate cortex. *J Neurosci* 3:1389–1413 [PubMed: 6864254]
- Bragg EM, Briggs F (2017) Large-scale reconstructions and independent, unbiased clustering based on morphological metrics to classify neurons in selective populations. *J vis Exp* 120:1–10
- Bragg EM, Fairless EA, Liu S, Briggs F (2017) Morphology of visual sector thalamic reticular neurons in the macaque monkey suggests retinotopically-specialized, parallel stream-mixed input to the lateral geniculate nucleus. *J Comp Neurol* 525:1273–1290 [PubMed: 27778378]
- Briggs F (2020) Role of feedback connections in central visual processing. *Annu Rev vis Sci* 6:18.1–18.22
- Briggs F, Kiley CW, Callaway EM, Usrey WM (2016) Morphological substrates for parallel streams of corticogeniculate feedback originating in both V1 and V2 of the macaque monkey. *Neuron* 90:388–399 [PubMed: 27041497]
- Briggs F, Usrey WM (2005) Temporal properties of feedforward and feedback pathways between thalamus and visual cortex in the ferret. *Thalamus Relat Syst* 3:133–139 [PubMed: 18176624]
- Briggs F, Usrey WM (2007) A fast, reciprocal pathway between the lateral geniculate nucleus and visual cortex in the macaque monkey. *J Neurosci* 27:5431–5436 [PubMed: 17507565]
- Briggs F, Usrey WM (2009) Parallel processing in the corticogeniculate pathway of the macaque monkey. *Neuron* 62:135–146 [PubMed: 19376073]
- Calinski T, Harabasz J (1974) A dendrite method for cluster analysis. *Commun Stat Theory Methods* 3:1–27
- Callaway EM (2005) Structure and function of parallel pathways in the primate early visual system. *J Physiol* 566:13–19 [PubMed: 15905213]
- Cauli B, Porter JT, Tsuzuki K, Lambalez B, Rossier J et al. (2000) Classification of fusiform neocortical interneurons based on unsupervised clustering. *PNAS* 97:6144–6149 [PubMed: 10823957]

- Conley M, Friederich-Ecsy B (1993) Functional organization of the ventral lateral geniculate complex of the tree shrew (*Tupaia belangeri*): II. Connections with the cortex, thalamus, and brainstem. *J Comp Neurol* 328:21–42 [PubMed: 7679121]
- Conley M, Raczkowski D (1990) Sublaminar organization within layer 6 of the striate cortex in galago. *J Comp Neurol* 302:425–436 [PubMed: 1705271]
- Cowey A (2010) Visual system: how does blindsight arise? *Curr Biol* 20:R702–R704 [PubMed: 20833309]
- Dell L-A, Innocenti GM, Hilgetag CC, Manger PR (2018) Cortical and thalamic connectivity of occipital visual cortical areas 17, 18, 19, and 21 of the domestic ferret (*Mustela putorius furo*). *J Comp Neurol* 527:1293–1314
- Dreher B, Michalski A, Ho RH, Lee CW, Burke W (1993) Processing of form and motion in area 21a of cat visual cortex. *Vis Neurosci* 10:93–115 [PubMed: 8424929]
- Felleman DJ, Van Essen DC (1991) Distributed hierarchical processing in the primate cerebral cortex. *Cereb Cortex* 1:1–47 [PubMed: 1822724]
- Fitzgibbon T, Bittar RG, Dreher B (1999) Projections from striate and extrastriate visual cortices of the cat to the reticular thalamic nucleus. *J Comp Neurol* 410:467–488 [PubMed: 10404413]
- Fitzpatrick D, Usrey WM, Schofield BR, Einstein G (1994) The sub-laminar organization of corticogeniculate neurons in layer 6 of macaque striate cortex. *Visual Neurosci* 11:307–315
- Gilbert CD, Kelly JP (1975) The projections of cells in different layers of the cat's visual cortex. *J Comp Neurol* 163:81–106 [PubMed: 1159112]
- Girard P, Salin PA, Bullier J (1992) Response selectivity of neurons in area MT of the macaque monkey during reversible inactivation of area V1. *J Neurophysiol* 67:1437–1446 [PubMed: 1629756]
- Grant S, Hilgetag CC (2005) Graded classes of cortical connections: quantitative analyses of laminar projections to motion areas of cat extrastriate cortex. *Eur J Neurosci* 22:681–696 [PubMed: 16101750]
- Grieve KL, Sillito AM (1995) Differential properties of cells in the feline primary visual cortex providing the corticofugal feedback to the lateral geniculate nucleus and visual claustrum. *J Neurosci* 15:4868–4874 [PubMed: 7623117]
- Harvey AR (1978) Characteristics of corticothalamic neurons in area 17 of the cat. *Neurosci Lett* 7:177–181 [PubMed: 19605109]
- Hasse JM, Bragg EM, Murphy AJ, Briggs F (2019) Morphological heterogeneity among corticogeniculate neurons in ferrets: quantification and comparison with a previous report in macaque monkeys. *J Comp Neurol* 527:546–557 [PubMed: 29664120]
- Hasse JM, Briggs F (2017a) Corticogeniculate feedback sharpens the temporal precision and spatial resolution of visual signals in the ferret. *Proc Natl Acad Sci USA* 114:E6222–E6230 [PubMed: 28698363]
- Hasse JM, Briggs F (2017b) A cross-species comparison of corticogeniculate structure and function. *Vis Neurosci* 34:1–9
- Hendrickson AE, Wilson JR, Ogren MP (1978) The neuroanatomical organization of pathways between the dorsal lateral geniculate nucleus and visual cortex in the old world and new world primates. *J Comp Neurol* 182:123–136 [PubMed: 100530]
- Homman-Ludiyé J, Manger PR, Bourne JA (2010) Immunohisto-chemical parcellation of the ferret (*Mustela putorius*) visual cortex reveals substantial homology with the cat (*Felis catus*). *J Comp Neurol* 518:4439–4462 [PubMed: 20853515]
- Humphrey AL, Sur M, Uhlrich DJ, Sherman SM (1985a) Projection patterns of individual X- and Y-cell axons from the lateral geniculate nucleus to cortical area 17 in the cat. *J Comp Neurol* 233:159–189 [PubMed: 3973100]
- Humphrey AL, Sur M, Uhlrich DJ, Sherman SM (1985b) Termination patterns of individual X- and Y-cell axons in the visual cortex of the cat: projections to area 18, to the 17/18 border region, and to both areas 17 and 18. *J Comp Neurol* 233:190–212 [PubMed: 3973101]
- Hupfeld D, Distler C, Hoffmann KP (2007) Deficits of visual motion perception and optokinetic nystagmus after posterior suprasylvian lesions in the ferret (*Mustela putorius furo*). *Exp Brain Res* 182:509–523 [PubMed: 17593360]

- Ichida JM, Mavity-Hudson JA, Casagrande VA (2014) Distinct patterns of corticogeniculate feedback to different layers of the lateral geniculate nucleus. *Eye Brain* 6:57–73
- Jackson CA, Hickey TL (1985) Use of ferrets in studies of the visual system. *Lab Anim Sci* 35:211–215 [PubMed: 3894786]
- Jarosiewicz B, Schummers J, Malik WQ, Brown EN, Sur M (2012) Functional biases in visual cortex neurons with identified projections to higher cortical targets. *Curr Biol* 22:269–277 [PubMed: 22305753]
- Jayakumar J, Roy S, Dreher B, Martin PR, Vidyasagar TR (2013) Multiple pathways carry signals from short-wavelength-sensitive ('blue') cones to the middle temporal area of the macaque. *J Physiol* 591:339–352 [PubMed: 23070701]
- Jones EG (2002) Thalamic organization and function after Cajal. *Prog Brain Res* 136:333–357 [PubMed: 12143393]
- Kaplan E (2004) The M, P, and K pathways of the primate visual system. In: Chalupa L, Werner J (eds) *The Visual Neurosciences*. MIT Press, Cambridge, pp 481–493
- Katz LC (1987) Local circuitry of identified projection neurons in cat visual cortex brain slices. *J Neurosci* 7:1223–1249 [PubMed: 3553446]
- Lempel AA, Nielsen KJ. 2019. Ferrets as a Model for Higher-Level Visual Motion Processing. *Curr Biol* 29: 179–91 e5 [PubMed: 30595516]
- Li B, Li BW, Chen Y, Wang LH, Diao YC (2000) Response properties of PMLS and PLLS neurons to simulated optic flow patterns. *Eur J Neurosci* 12:1534–1544 [PubMed: 10792431]
- Lin CS, Kaas JH (1977) Projections from cortical visual areas 17, 18, and MT onto the dorsal lateral geniculate nucleus in owl monkeys. *J Comp Neurol* 173:457–474 [PubMed: 404339]
- Lund JS, Boothe RG (1975) Interlaminar connections and pyramidal neuron organization in the visual cortex, area 17, of the macaque monkey. *J Comp Neurol* 159:305–334
- Lund JS, Lund RD, Hendrickson AE, Bunt AH, Fuchs AF (1975) The origin of efferent pathways from the primary visual cortex, area 17, of the macaque monkey as shown by retrograde transport of horseradish peroxidase. *J Comp Neurol* 164(287):303
- Lyon DC, Rabideau C (2012) Lack of robust LGN label following transneuronal rabies virus injections into macaque area V4. *J Comp Neurol* 520:2500–2511 [PubMed: 22237967]
- Lysakowski A, Standage GP, Benevento LA (1988) An investigation of collateral projections of the dorsal lateral geniculate nucleus and other subcortical structures to cortical areas V1 and V4 in the macaque monkey: a double label retrograde tracer study. *Exp Brain Res* 69:651–661 [PubMed: 2836233]
- Michalski A, Wimborne BM, Henry GH (1993) The effect of reversible cooling of cat's primary visual cortex on the responses of area 21a neurons. *J Physiol* 466:133–156 [PubMed: 8410689]
- Osakada F, Mori T, Cetin A, Marshel JH, Virgen B, Callaway EM (2011) New rabies virus variants for monitoring and manipulating activity and gene expression in defined neural circuits. *Neuron* 71:617–631 [PubMed: 21867879]
- Philipp R, Distler C, Hoffmann KP (2006) A motion-sensitive area in ferret extrastriate visual cortex: an analysis in pigmented and albino animals. *Cereb Cortex* 16:779–790 [PubMed: 16135782]
- Radtke-Schuller S (2018) *Cyto- and myeloarchitectural brain atlas of the ferret (Mustela putorius) in MRI aided stereotaxic coordinates*. Springer Press, New York
- Rockland KS (1994) Further evidence for two types of corticopulvinar neurons. *NeuroReports* 5(1865):68
- Rodman HR, Gross CG, Albright TD (1989) Afferent basis of visual response properties in area MT of the macaque. I. Effects of striate cortex removal. *J Neurosci* 9:2033–2050 [PubMed: 2723765]
- Rosa MGP, Tweedale R, Elston GN (2000) Visual responses of neurons in the middle temporal area of new world monkeys after lesions of striate cortex. *J Neurosci* 20:5552–5563 [PubMed: 10884339]
- Schmid MC, Mrowka SW, Turchi J, Saunders RC, Wilke M et al. (2010) Blindsight depends on the lateral geniculate nucleus. *Nature*
- Sherk H (1986) Coincidence of patchy inputs from the lateral geniculate complex and area 17 to the cat's Clare-Bishop area. *J Comp Neurol* 253:105–120 [PubMed: 2432097]

- Sherman SM, Guillery RW (2006) Exploring the thalamus and its role in cortical function. MIT Press, Boston
- Sincich LC, Park KF, Wohlgemuth MJ, Horton JC (2004) Bypassing V1: a direct geniculate input to area MT. *Nat Neurosci* 7:1123–1128 [PubMed: 15378066]
- Talebi V, Baker CI (2016) Categorically distinct types of receptive fields in early visual cortex. *J Neurophysiol* 115:2556–2576 [PubMed: 26936978]
- Thorndike RL (1953) Who belongs in the family? *Psychometrika* 18:267–276
- Tong L, Kalil RE, Spear PD (1982) Thalamic projections to visual areas of the middle suprasylvian sulcus in the cat. *J Comp Neurol* 212:103–117 [PubMed: 6321560]
- Tsumoto T, Suda K (1980) Three groups of cortico-geniculate neurons and their distribution in binocular and monocular segments of cat striate cortex. *J Comp Neurol* 193:223–236 [PubMed: 7430428]
- Usrey WM, Fitzpatrick D (1996) Specificity in the axonal connections of layer 6 neurons in tree shrew striate cortex: evidence for distinct granular and supragranular systems. *J Neurosci* 16:1203–1218 [PubMed: 8558249]
- Wang C, Waleszczyk WJ, Burke W, Dreher B (2000) Modulatory influence of feedback projections from area 21a on neuronal activities in striate cortex of the cat. *Cereb Cortex* 10:1217–1232 [PubMed: 11073871]
- Weiskrantz L (2009) Is blindsight just degraded normal vision? *Exp Brain Res* 192:413–416 [PubMed: 18438650]
- Wickersham IR, Finke S, Conzelmann KK, Callaway EM (2007) Retrograde neuronal tracing with a deletion-mutant rabies virus. *Nat Methods* 4:47–49 [PubMed: 17179932]

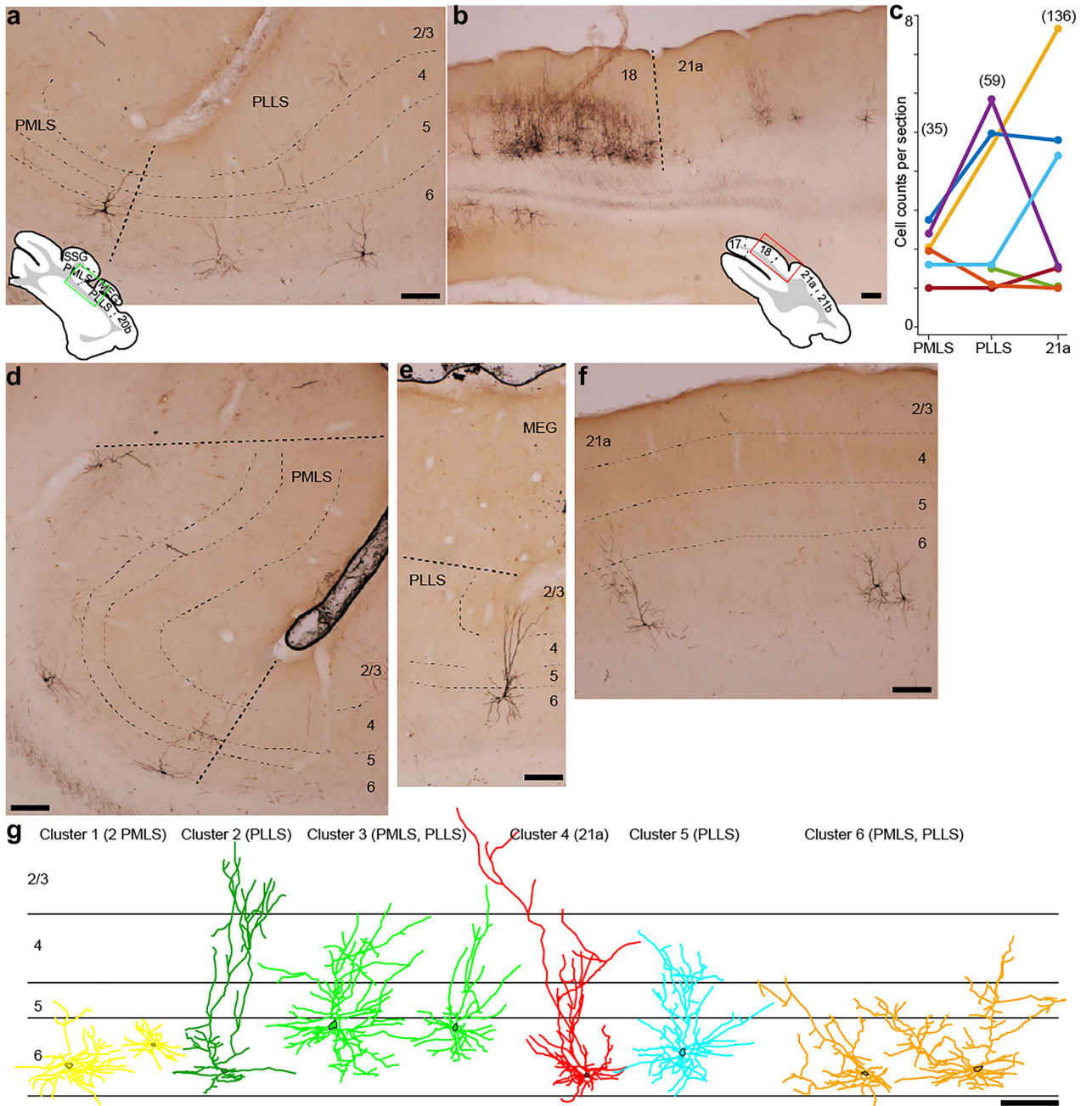


Fig. 1. Virus-labeled corticogeniculate neurons in extrastriate areas PMLS, PLLS, and 21a. **a** Coronal section showing PMLS and PLLS. Green box in inset illustrates region of image. Layers are indicated by thin dashed lines and labeled at right; thicker dashed line indicates border between areas. Scale bars represent 200 μm for all panels. **b** Lower magnification coronal section showing areas 18 and 21a. Red box in inset illustrates region of image; dashed line indicates area border. **c** Counts of virus-labeled corticogeniculate neurons per area, normalized by number of sections per area. Colors represent individual ferrets. Numbers above indicate total corticogeniculate cell counts per area across all ferrets.

Author Manuscript

Author Manuscript

Author Manuscript

Author Manuscript

d–f Higher magnification coronal sections through PMLS (**d**), PLLS (**e**) and 21a (**f**) illustrating dendritic fields of virus-labeled corticogeniculate neurons. Conventions as in **a. g** Representative examples of reconstructed dendritic arbors of corticogeniculate neurons in each of the six clusters (color coded as in Figs. 2 and 3). Area of origin of each reconstructed neuron listed at top. Cell bodies are indicated by black outlines. Scale bar representing 200 μm is an estimate as individual reconstructions were scaled to fit approximate laminar boundaries

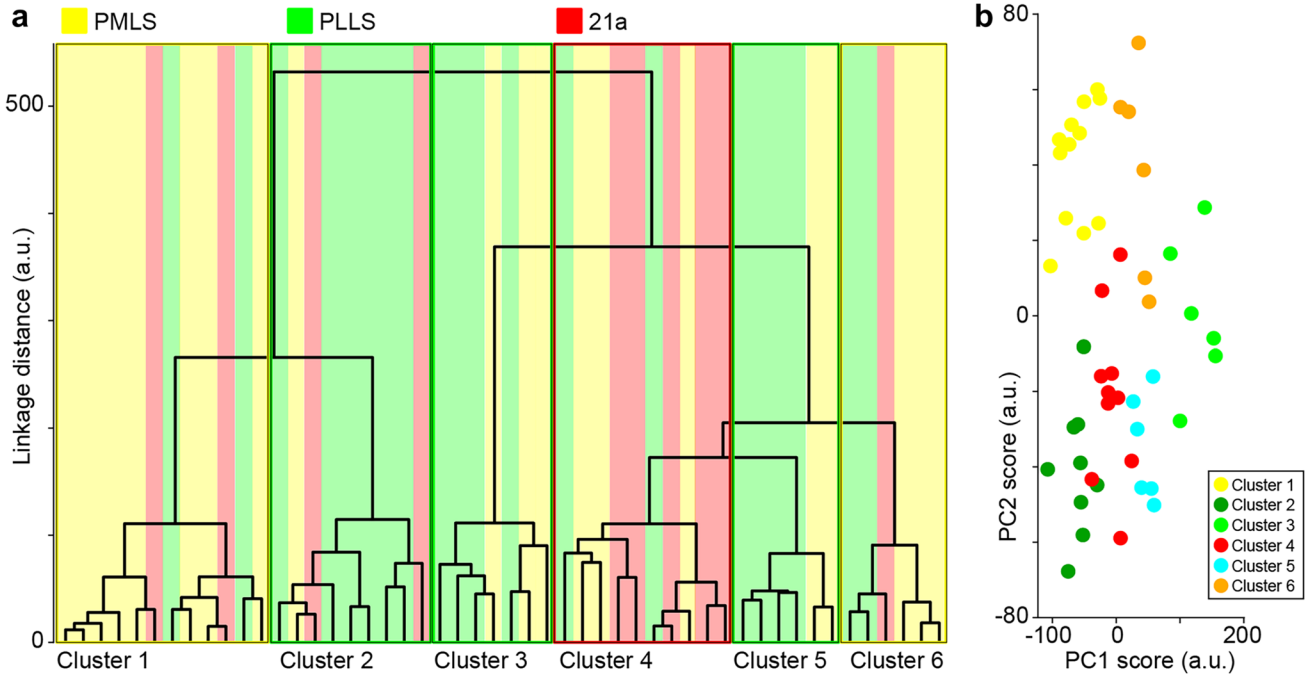


Fig. 2. Clustering of extrastriate corticogeniculate neurons. **a** Dendrogram of linkage distances (arbitrary units) between individual corticogeniculate neurons based on 14 independent morphological metrics (Tables 1, 2 and 3). Colors indicate extrastriate area of origin of each corticogeniculate neuron: yellow indicates PMLS, green indicates PLLS, and red indicates 21a. Clusters indicated by thin boxes with colored outlines representing the area of origin of the majority of neurons per cluster. **b** Results of a separate PCA analysis of the same 14 morphological metrics used in the cluster analysis with neurons color coded by their assignment from the cluster analysis. PC1 and PC2 scores (arbitrary units) are the representations in 14-dimensional space for the first and second principal components, respectively

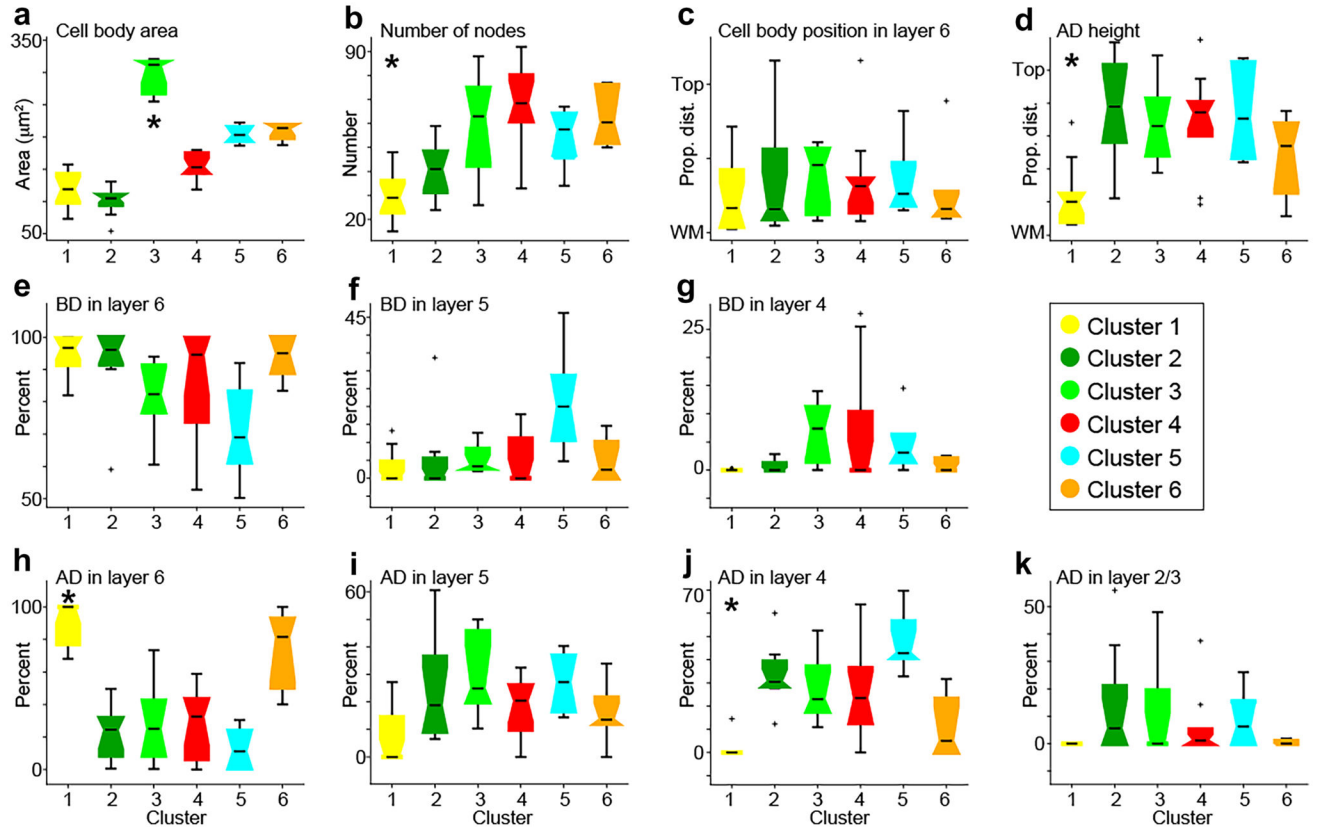


Fig. 3. Statistical comparisons of morphological metrics across extrastriate corticogeniculate neurons in each cluster. Clusters are color coded according to the legend middle right. Notched box and whisker plots illustrate the median (horizontal black lines), the 25th and 75th percentiles (notched boxes), data distributions (black lines above, below boxes), and outliers (black crosses). Asterisks indicate statistically significant differences across clusters (see Tables 1, 2 and 3 for all statistics). **a** Cell body area. **b** Number of nodes. **c** Cell body position in layer 6 with top indicating the layer 5/6 border and WM indicating the white matter boundary. **d** Height of the apical dendrite (AD) with top indicating the top of layer 2/3 and WM indicating the white matter boundary. **e–g** Percentage of basal dendrite (BD) in layers 6 (**e**), 5 (**f**), and 4 (**g**). **h–k** Percentage of apical dendrite (AD) in layers 6 (**h**), 5 (**i**), 4 (**j**), and 2/3 (**k**)

Table 1

Average \pm SEM for 5 morphological metrics included in the cluster analysis: cell body (CB) area and roundness, total number of nodes, cell body position in layer 6 (L6), and height of the apical dendrite (AD)

	CB area	CB roundness	# Nodes	CB pos. in L6	AD height
Cluster 1 ($n = 12$)	119 \pm 8.1	0.6 \pm 0.03	30 \pm 2.9	0.8 \pm 0.055	0.78 \pm 0.06
Cluster 2 ($n = 9$)	100.5 \pm 7.9	0.56 \pm 0.03	40.8 \pm 3.8	0.7 \pm 0.12	0.24 \pm 0.11
Cluster 3 ($n = 7$)	295.1 \pm 11.3	0.55 \pm 0.03	58.6 \pm 8.8	0.7 \pm 0.08	0.33 \pm 0.1
Cluster 4 ($n = 10$)	155 \pm 6.2	0.57 \pm 0.05	67.9 \pm 5.7	0.72 \pm 0.08	0.31 \pm 0.1
Cluster 5 ($n = 6$)	204.2 \pm 6.2	0.56 \pm 0.08	54.3 \pm 5.7	0.71 \pm 0.09	0.26 \pm 0.13
Cluster 6 ($n = 6$)	208.7 \pm 5.7	0.56 \pm 0.07	62.7 \pm 5.2	0.77 \pm 0.11	0.52 \pm 0.11
<i>p</i> values	5.76 $\times 10^{-8}$	0.96	4.39 $\times 10^{-5}$	0.704	0.0016
Differences	3 > all		1 < 3,4,6; 2 < 4		1 > 2, 4, 5

Smaller number for CB position and height indicate closer to the pia. *p* values in bold text indicate statistical differences across clusters with specific differences listed below

Table 2

Average \pm SEM for 5 morphological metrics included in the cluster analysis: percent of apical dendrite (AD) in each layer

	AD in L6	AD in L5	AD in L4	AD in L2/3	AD above L2/3
Cluster 1 ($n = 12$)	91.4 \pm 3.9	6.8 \pm 3.3	1.2 \pm 1.3	0	0
Cluster 2 ($n = 9$)	21.9 \pm 5.8	25.2 \pm 7.2	33.4 \pm 4.6	14.2 \pm 6.96	2.0 \pm 1.55
Cluster 3 ($n = 7$)	28.4 \pm 10.4	30.3 \pm 6.2	27.3 \pm 5.95	11.4 \pm 7.4	0.4 \pm 0.5
Cluster 4 ($n = 10$)	27.7 \pm 7.6	17.4 \pm 3.9	25.1 \pm 6.8	6.2 \pm 3.95	2.8 \pm 2.9
Cluster 5 ($n = 6$)	13.0 \pm 5.5	27.1 \pm 4.7	47.6 \pm 6.0	9.0 \pm 4.85	0.8 \pm 0.6
Cluster 6 ($n = 6$)	74.5 \pm 10.8	15.8 \pm 5.1	10.8 \pm 6.1	0.5 \pm 0.4	0
<i>p</i> values	3.52×10^{-6}	0.011	1.43×10^{-5}	0.065	0.22
Differences	1 < 2–5; 6 < 5		1 < 2–5; 6 < 5		

p values in bold text indicate statistical differences across clusters with specific differences listed below

Table 3

Average \pm SEM for 4 morphological metrics included in the cluster analysis: percent of basal dendrite (BD) in each layer and the white matter (WM)

	BD in WM	BD in L6	BD in L5	BD in L4
Cluster 1 ($n = 12$)	2.5 \pm 1.5	94.8 \pm 1.9	2.7 \pm 1.4	0.03 \pm 0.03
Cluster 2 ($n = 9$)	2.1 \pm 0.9	92.1 \pm 4.6	5.2 \pm 3.9	0.6 \pm 0.4
Cluster 3 ($n = 7$)	1.8 \pm 0.7	81.8 \pm 4.7	5.7 \pm 1.65	7.1 \pm 2.2
Cluster 4 ($n = 10$)	2.4 \pm 0.9	86.3 \pm 5.7	4.8 \pm 2.3	6.6 \pm 3.7
Cluster 5 ($n = 6$)	2.3 \pm 0.8	70.8 \pm 6.7	21.7 \pm 6.9	4.7 \pm 2.4
Cluster 6 ($n = 6$)	0.6 \pm 0.5	93.7 \pm 3.2	4.9 \pm 2.8	0.8 \pm 0.5
<i>p</i> values	0.358	0.013	0.019	0.0098

p values in bold text indicate statistical differences across clusters with specific differences listed below